IL NUOVO CIMENTO **42 C** (2019) 237
DOI 10.1393/ncc/i2019-19237-0

COMMUNICATIONS: SIF Congress 2018

Imaging detectors based on photoluminescence of radiation-induced defects in lithium fluoride for XFEL beam monitoring

F. BONFIGLI([1]) on behalf of F. CAPOTONDI([2]), A. CRICENTI([3]), L. GIANNESSI([1]), M. KISKINOVA([2]), M. LUCE([3]), N. MAHNE([2])([4]), M. MANFREDDA([2]), R. M. MONTEREALI([1]), E. NICHELATTI([5]), E. PEDERSOLI([2]), L. RAIMONDI([2]), M. A. VINCENTI([1]), M. ZANGRANDO([2])([4])

([1]) *ENEA C.R. Frascati, Fusion and Technologies for Nuclear Safety and Security Dept. V. E. Fermi, 45, 00044, Frascati, Rome, Italy*
([2]) *Elettra Sincrotrone Trieste S.C.p.A. - Strada Statale 14, 34149, Basovizza, Trieste, Italy*
([3]) *Istituto di Struttura della Materia (ISM-CNR) - V. del Fosso del Cavaliere 100, Rome, 00133, Italy*
([4]) *Istituto Officina dei Materiali (IOM-CNR) - Strada Statale 14, 34149, Basovizza, Trieste, Italy*
([5]) *ENEA C.R. Casaccia, Fusion and Technologies for Nuclear Safety and Security Dept. V. Anguillarese, 301, 00123, S. Maria di Galeria, Rome, Italy*

received 8 March 2019

Summary. — Lithium fluoride (LiF) films and crystals are versatile X-ray imaging detectors based on the optical reading of visible photoluminescence from radiation-induced electronic defects. Distinctive features of these detectors are their high spatial resolution across a large field of view, wide dynamic range and insensitivity to ambient light. These peculiarities of LiF detectors appear to be promising for monitoring the spatial intensity distribution of ultra-short, ultra-high pulses of the EUV-X-ray Free Electron Laser (XFEL) and could be exploited for coherent diffraction imaging experiments.

1. – Introduction

Point defects —impurity ions, color centers (CCs), etc.— in insulating materials [1,2] are successfully used for radiation detectors [3]. Although impressive advances in electronic design and direct detection materials continue to drive progress in the development of radiation imaging detectors, the role of luminescent materials is still of relevance in this field [4]. Pure and doped alkali halide crystals containing CCs represent one of the most investigated fields in solid state physics with relevance to optical properties [5]. Novel lithium fluoride (LiF) X-ray imaging detectors are based on the optical reading of visible photoluminescence (PL) from radiation-induced electronic defects, known as

CCs [6]. In LiF, stable CCs can be produced by ionizing radiations, such as charged particles, *e.g.*, high-energy ions [7] and electrons [8], energetic photons, like X-rays [9] and γ-rays [10]. Among alkali halides, LiF has several peculiar physical and optical properties as follows: i) in spite of its typical ionic structure, the crystal is resistant to moisture (0.13 g/100 g H_2O solubility) and relatively hard (Knupp hardness 99 Kg/mm^2); ii) characterized by a face-centered cubic (f.c.c.) structure, with the shortest nearest-neighbor distance of 0.2013 nm; iii) the Li^+ cation and the F^- anion have the smallest radii, 0.06 and 0.136 nm, respectively; iv) LiF band gap, about 14 eV [11], is the largest one among any common solids; v) its refractive index, about 1.39 in the visible spectral range [12], is among the lowest ones for solid dielectric materials; vi) transparent in the wavelength range from $\sim$120 nm to 7 μm and it is commonly used as window material in pure form, especially in the ultraviolet (UV) due to its high transmission.

Among the radiation-induced CCs created in LiF, F_2 and F_3^+ defects, which consist of two electrons bound to two and three close anion vacancies, respectively, are optically active with broad absorption and emission bands in the visible spectral range [13]. These defects have almost overlapping broad absorption bands (M-band) peaked at about 450 nm [13] and, therefore, they can be simultaneously excited with a single pump wavelength in the blue spectral interval. On the other hand, they exhibit two different Stokes-shifted broad emission bands in the green (F_3^+) and red (F_2) spectral ranges [13]. Figure 1 reports the room temperature (RT) normalized absorption and emission bands of F_2 and F_3^+ CCs.

The operation principle of a passive LiF radiation imaging detector is based on the detection of the PL emitted by F_2 and F_3^+ CCs locally produced during the irradiation process. A scheme of this operation process is depicted in fig. 2, where the detector is represented as a LiF film-based plate. The LiF film is exposed to X-rays, see fig. 2(a); the irradiation produces a layer of stable CCs, whose concentration is locally proportional to the absorbed dose. Lower X-ray doses correspond to the formation of lower CC densities in the colored layer, while higher X-ray doses induce higher CC densities. The depth of the colored layer is dependent on the X-ray energies, as will be detailed in the experimental section. After exposure, the stable X-ray image stored in the LiF film is

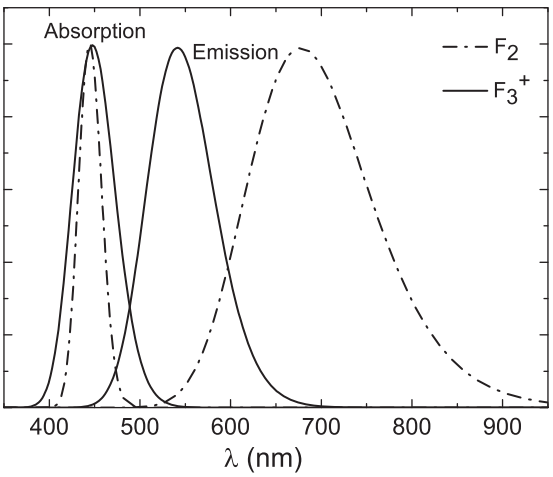

Fig. 1. – RT normalized absorption and emission bands of F_2 and F_3^+ CCs in LiF.

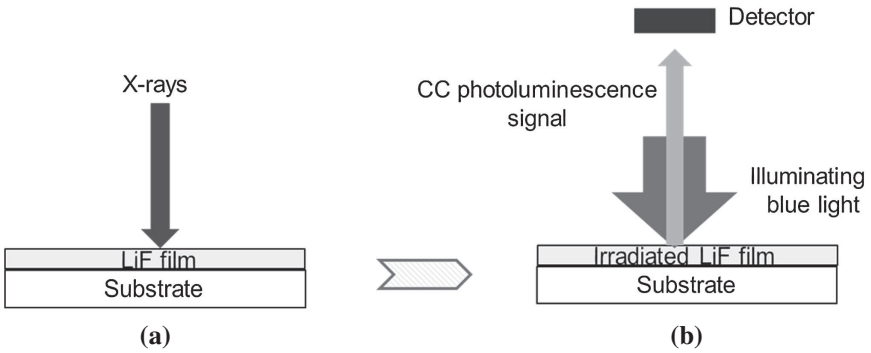

Fig. 2. – Scheme of LiF detector operation as X-ray imaging detector. (a) X-ray irradiation process and formation of CCs. (b) Readout process based on the detection of CCs visible PL signal from the irradiated LiF film detector under blue-light illumination.

read by illuminating it with blue light and detecting the red and green PL emitted by F_2 and F_3^+ CCs, see fig. 2(b). The optical readout process of LiF plates can directly be performed by means of an optical fluorescence microscope, which has to be equipped with a blue-light source, such as a filtered lamp or a blue LED or a blue laser, spectrally centered around the peak wavelength of the M-band to simultaneously excite the PL of F_2 and F_3^+ defects.

The main peculiarities of these LiF-based imaging detectors are an intrinsic very high spatial resolution, a large field of view and a wide dynamic range. The intrinsic spatial resolution of this detector is related to the size of CCs produced by X-rays, that is less than 1 nm [14]. In practice, the spatial resolution is limited by the optical microscope and the technique utilized for PL detection in the optical reading process. By using advanced fluorescence optical microscopes as readout instruments, like Confocal Laser Scanning Microscope (CLSM) or Scanning Near Field Optical Microscope (SNOM), optical fluorescence images with sub-micrometric [15] and nanometric spatial resolution [16], respectively, were obtained on LiF-based X-ray imaging detectors. Moreover, the LiF-based detectors are easy to handle, as insensitive to visible light, and no development process is needed. They allow for great versatility, since they can be grown in the form of thin films on different substrates by well-assessed physical deposition techniques, tailoring their appropriate geometry, size and thickness, allowing their integration in different experimental apparatus and configurations. The high quantum efficiency [17] of broad red and green photoemission bands from F_2 and F_3^+ defects under blue pumping together with the LiF optical transparency allows for the use of optical fluorescence microscopy in the visible spectral range as a fast, sensitive and low-cost reading technique. These peculiar features make LiF radiation sensors based on the PL of CCs very attractive as solid state detectors for X-ray imaging applications.

The opportunity to perform imaging in the extreme UV (EUV), soft and hard X-ray spectral range (photon energies 20 eV–30 keV), with a very high spatial resolution across a wide field of view, is considered a topical task nowadays. Indeed, the fast development of different types of intense laboratory-EUV and soft X-ray sources, like Laser Plasma Produced (LPP) sources, X-ray lasers, etc., as well as powerful and compact X-ray tubes and the availability of large scale facilities like synchrotrons and FEL, makes radiation imaging applications very attractive in physics and in life sciences. In particular, in the

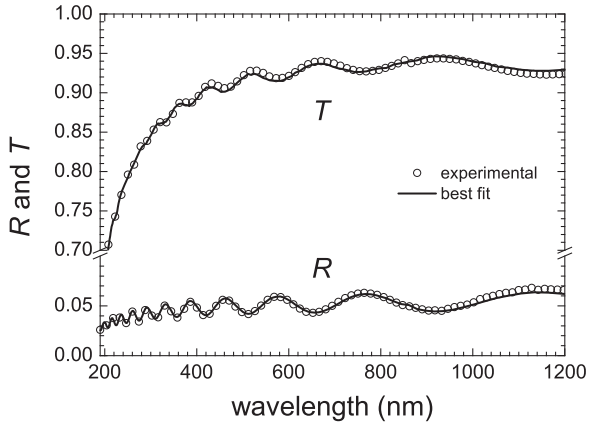

Fig. 3. – Reflectance and transmittance spectra of non-irradiated LiF film grown on silica substrate measured at room temperature together with the best fit curves.

(2.2–4.4) nm wavelength interval, known as water-window, water is much less absorbing than organic compounds, such as proteins and carbohydrates, containing carbon. Therefore, images with a natural contrast can be obtained for specimens containing water [18]. The LiF X-ray imaging detectors were successfully tested by using several X-ray sources, like synchrotrons [19, 20], LPP sources [9, 21, 22], capillary discharge lasers [23], X-ray tubes [16, 24]. X-ray micro-radiographies of biological samples, even *in vivo* specimens [21], geological samples [24] and geometric nano-structures were obtained in absorption-contrast configuration, mainly performed in contact mode, and in phase-contrast configurations [25], both in the soft and hard X-ray spectral ranges.

The diagnostics of an ultra-short, ultra-bright focused XFEL beam in terms of beam size in free propagation or after a focusing system, is critical for all XFEL experiments. Complex and/or time-consuming methods are currently used to determine the XFEL beam parameters: grating interferometers, knife-edge scan methods, wavefront sensors. Routine characterization of XUV-FEL focal spots mainly relies on the surface damage of organic polymers. In particular, ablation craters in PMMA (polymethyl methacrylate) are used to estimate the beam profile and the beam diameter of focal spots [26]. For XUV/soft X-ray laser beams, optical microscope and atomic force microscope (AFM) images of ablated craters allow reconstructing the major part of the transverse time-integrated intensity distribution for intensities up to the limiting PMMA threshold fluence. Also LiF crystals were used as CCs-based imaging detectors with soft X-ray pulses of SASE FEL [27] and with hard X-ray pulses for visualization of XFEL beam and for phase contrast imaging [28-30]. In this paper, we report the first results for the detection of ultra-short, ultra-intense pulses provided by the FERMI-FEL [31] using LiF films. Thermally evaporated LiF thin films were irradiated with focused FEL pulses of $\lambda = 32$ nm at different fluences. The stored images were read by a confocal laser scanning microscope in fluorescence mode.

2. – Experimental and results

Optically transparent polycrystalline LiF thin films were grown by thermal evaporation on amorphous (*i.e.*, glass and silica) substrates in controlled conditions at the

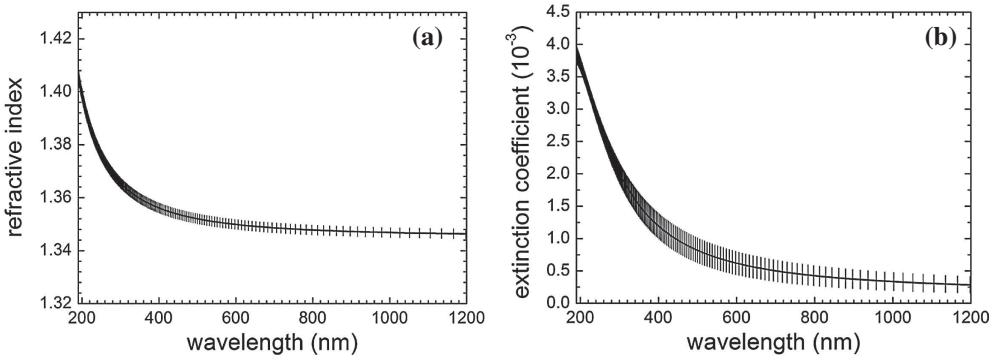

Fig. 4. – Obtained refractive index (a) and extinction coefficient (b) of the LiF film grown on silica substrate.

Photonic Micro- and Nano-structures Laboratory (FSN-TECFIS-MNF) of ENEA C.R. Frascati.

The structural, morphological and optical properties of LiF thin films strongly depend on the depositions parameters such as pressure and nature of residual gas in deposition chamber, deposition rate, substrate temperature, nature of substrate (amorphous, poly-crystalline or mono-crystalline) and total thickness. A thermally evaporated LiF thin film on a glass substrate with thickness of about 850 nm was used as imaging plate to detect the focused FEL beam. This LiF film was grown under vacuum (10^{-4}–10^{-5} Pa), with a temperature of the substrate of 300 °C and a deposition rate of 1 nm/s. A LiF film grown on silica substrate in the same deposition run was characterized by spectrophotometric measurements (transmittance T and reflectance R) in the wavelength range of (190–1600) nm in order to obtain with a fitting procedure the spectral dispersions of its refractive index n and extinction coefficient k [32]. Figure 3 reports the measured R and T spectra acquired at RT together with the best fit curves of the not irradiated LiF film. The procedure provided the best fitting spectral dispersions of n and k, shown in fig. 4, and also the thickness of (854 ± 5) nm and the very small refractive index gradient $(-0.5 \pm 0.3)\%$, indicating a good refractive index homogeneity along the film thickness.

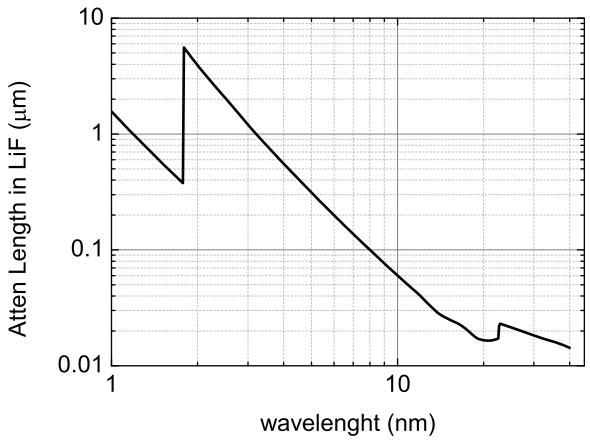

Fig. 5. – Attenuation length of X-rays in LiF [35].

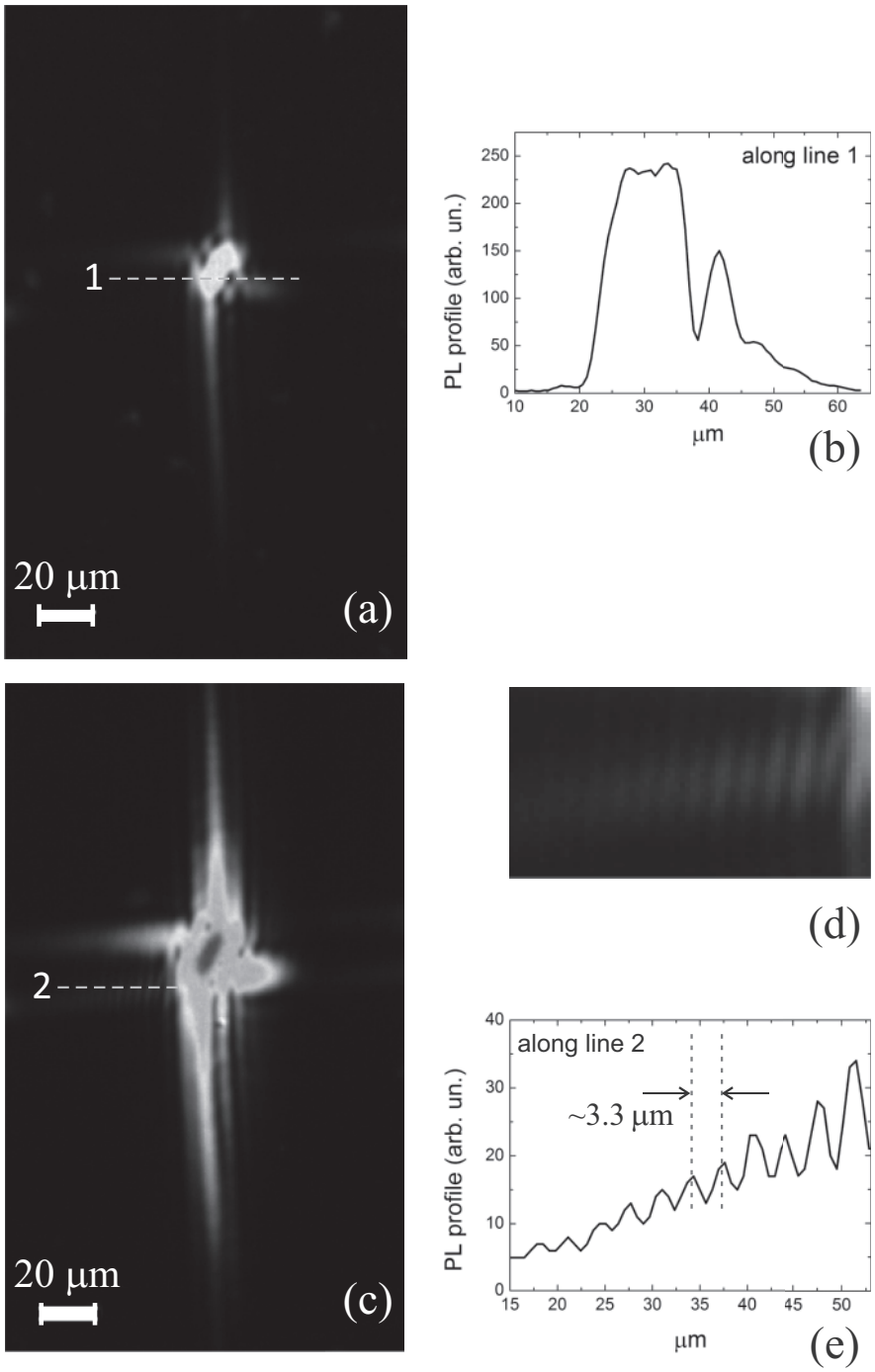

Fig. 6. – CLSM fluorescence images of focused FERMI XFEL beams at two different fluences: $F = 75\,\mathrm{mJ/cm^2}$ (a) and $F = 750\,\mathrm{mJ/cm^2}$ (c) stored by CCs in a LiF film. (b) PL intensity profile along line 1 of (a). (d) Enlarged view of a diffraction pattern along the line 2 in (c). (e) PL intensity profile of the diffraction pattern along the line 2 in (c).

At the visible wavelengths, where the F_2 and F_3^+ PL bands are located, the refractive index is almost constant and the extinction coefficient is below 10^{-3}, assuring enough transparency for limited thicknesses.

A LiF film of diameter 10 mm grown on glass substrate $(12 \times 12 \times 1)\,\mathrm{mm}^3$ was irradiated under vacuum with single-shot focused FEL beam at FERMI (FEL1, $\lambda = 32\,\mathrm{nm}$, 60 fs) at different fluences ranging from $75\,\mathrm{mJ/cm^2}$ to $750\,\mathrm{mJ/cm^2}$ by moving the sample after each shot. FERMI FEL is a laser-seeded user-facility covering the spectral range from 100 nm (12 eV) to 4 nm (320 eV) [31]. Based on the high gain harmonic generation scheme, FERMI provides users with photon pulses of 50–100 fs. The experiments were performed at DiProI (Diffraction Projection Imaging) beamline [33]. During the experiments, the XFEL beam was focused by bendable planar mirrors in Kirkpatrick-Baez configuration [34] (focal length 1.2–1.75 m, photon flux 1×10^{12} ph/pulse at 5 nm, minimum spot size $(3 \times 5)\,\mu\mathrm{m}^2$).

The X-ray penetration in solids is strongly dependent on the photon energy. Figure 5 shows the attenuation length of X-rays in LiF [35]. In the EUV (20–200) eV it results of a few tens of nanometers, it raises to several micrometers in the soft X-rays region (200 eV–2 keV), depending on the selected energy, and reaches up to 100 μm and more at higher energies. In particular, for the used FEL emission wavelength, that is 32 nm, the corresponding attenuation length in LiF is estimated about 17 nm, which is well below the thickness of the used LiF film detector.

The fluorescence images of the single-shot focused XFEL beams stored in the LiF film was read by a CLSM equipped with a CW argon laser at 457.9 nm. The F_2 and F_3^+ CC PL signals were simultaneously detected by a system of two photomultipliers. Figures 6(a) and (c) show the CC fluorescence images detected by CLSM of the FEL beams at the minimum and maximum used fluences. Even at the lowest fluence, the spot image is clearly visible despite of the limited thickness of the colored layers. High-resolution details of the focused FEL beam are well visible. Figure 6(b) reports the PL intensity profile along the line 1 of fig. 6(a). Figure 6(d) shows an enlarged view (with enhanced luminosity and contrast performed by software) of a diffraction pattern located in the spot of fig. 6(c) along the line 2. The PL intensity profile along the line 2 is reported in fig. 6(e). These interference effects, outside the main beam spot, are due to the finite size of the KB optics and high degree of coherence of FEL radiation. From the PL profile of the graph reported in fig. 6(d), a period of $\sim$3.3 μm of the diffraction pattern has been derived. This interference fringes provide information on the entrance angle of the radiation on the KB optics, that was estimated $\sim$2–2.5 deg. In the spot at the highest fluence, a darker luminescent central area appears (see fig. 6(b)) corresponding to the brighter part of the XFEL beam. It could be due to a structural damage of the LiF film surface or to more complex phenomena, as photoluminescence quenching for the formation of larger aggregated defects due to a local high density of CCs. Further investigations are under way to study this aspect by using different microscopy techniques, such as SNOM and CLSM operating in fluorescence and reflection modes.

3. – Conclusions

A LiF thin film thermally evaporated on a glass substrate was used as X-ray imaging detector based on the optical reading of visible PL from radiation-induced stable electronic defects, for detecting the spatial intensity distribution of single-shot focused FERMI XFEL beam with emission wavelength at 32 nm and at different X-ray fluences. The images of the XFEL beam stored in the LiF film were read by an optical microscope

operating in fluorescence mode (confocal laser-scanning configuration). High-resolution details of the focused XFEL beam were detected. The obtained results are very promising for the use of LiF films as imaging detectors for monitoring the XFEL beam intensity distribution, for optimization of focusing systems, but also for coherent diffraction imaging experiments, requiring high-resolution and high dynamic range imaging detectors with a wide field of view, even for sequences of single shots.

REFERENCES

[1] Sthoneham A. M., *Theory of Defects in Solids* (Oxford University Press, Oxford) 1975.
[2] Fowler W. B., *Physics of Color Centers* (Academic Press, New York and London) 1968.
[3] Shionoya S. *et al.*, *Phosphor Handbook* (CRC Press, Boca Raton) 1998.
[4] Yukihara E. G. *et al.*, *Optically Stimulated Luminescence: Fundamentals and Applications* (Wiley) 2011.
[5] Schulman J. H. *et al.*, *Color Centers in Solids*, edited by Smoluchowski R. and Kurti N. (Pergamon Press, Oxford) 1963.
[6] Montereali R. M., *Nuovo Cimento C*, **36** (2013) 35.
[7] Perez A. *et al.*, *Nucl. Instrum. Methods*, **132** (1976) 219.
[8] Baldacchini G. *et al.*, *Nucl. Instrum. Methods Phys. Res. B*, **191** (2002) 216.
[9] Baldacchini G. *et al.*, *Rev. Sci. Instrum.*, **76** (2005) 113104.
[10] Baldacchini G. *et al.*, *Phys. Rev. B*, **54** (1996) 2417508.
[11] Piacentini M., *Solid State Commun.*, **17** (1975) 697.
[12] Perez A. *et al.*, *Handbook of Optical Constants of Solids*, edited by Palik E. D. (Academic Press, New York) 1985.
[13] Nahum J. *et al.*, *Phys. Rev.*, **154** (1967) 817.
[14] Sekatski S. K. *et al.*, *Appl. Phys. B*, **63** (1996) 525.
[15] Ustione A. *et al.*, *Appl. Phys. Lett.*, **88** (2006) 141107.
[16] Almaviva S. *et al.*, *Appl. Phys. Lett.*, **89** (2006) 54102.
[17] Basiev T. *et al.*, *IEEE J. Quantum Electron.*, **24** (1998) 1052.
[18] Attwood D., *Soft X Rays and Extreme Ultraviolet Radiation: Principles and Applications* (Cambridge University Press, Cambridge, U.K.) 1999.
[19] Larciprete R. *et al.*, *Appl. Phys. Lett.*, **80** (2002) 3862.
[20] Bonfigli F. *et al.*, *Radiat. Meas.*, **56** (2013) 277.
[21] Bonfigli F. *et al.*, *Microsc. Res. Tech.*, **71** (2008) 35.
[22] Baldacchini G. *et al.*, *Appl. Phys. Lett.*, **80** (2002) 4810.
[23] Tomassetti G. *et al.*, *Appl. Phys. Lett.*, **85** (2004) 4163.
[24] Hampai D. *et al.*, *EPL*, **96** (2011) 60010.
[25] Nichelatti E. *et al.*, *Nucl. Instrum. Methods Phys. Res. A*, **833** (2016) 68.
[26] Chalupský J. *et al.*, *Opt. Express*, **15** (2007) 6036.
[27] Pikuz T. *et al.*, *Opt. Express*, **20** (2012) 3424.
[28] Pikuz T. *et al.*, *Sci. Rep.*, **8** (2018) 16407.
[29] Faenov A. Y. *et al.*, *Sci. Rep.*, **8** (2018) 16407.
[30] Pikuz T. *et al.*, *Matter Radiat. Extremes*, **3** (2018) 197.
[31] Allaria E. *et al.*, *Nat. Photon.*, **6** (2012) 699.
[32] Montecchi M. *et al.*, *Thin Solid Films*, **396** (2001) 264.
[33] Capotondi F. *et al.*, *Rev. Sci. Instrum.*, **84** (2013) 051301.
[34] Raimondi L. *et al.*, *Nucl. Instrum. Methods Phys. Res. A*, **710** (2013) 131.
[35] `http://henke.lbl.gov/optical_constants/atten2.html`.